

Dynamical Phase Diagrams for Moving Vortices Interacting with Periodic Pinning

Gilson Carneiro*

Instituto de Física

Universidade Federal do Rio de Janeiro

C.P. 68528

21945-970, Rio de Janeiro-RJ

Brasil

(October 28, 2018)

The dynamical phase diagrams for vortices in clean films, driven by an uniform force, and interacting with periodic pinning resulting from a columnar-defect lattice are investigated by numerical simulations of a London model, and other considerations. Dynamical phases are identified according to the spatial symmetry, and dynamical phase diagrams are studied as a function of the driving force magnitude and direction, and on the temperature, for typical vortex densities. The theoretical limit of infinite drive-force magnitudes is investigated first. In this limit vortex motion averages the periodic pinning potential in the direction of motion, and the dynamical phases reduce to thermal equilibrium ones for vortices interacting with the averaged pinning potential. For most directions of motion this potential is essentially constant. For a few particular ones it is a one-dimensional washboard, periodic in the direction transverse to motion. The dynamical phase diagrams in this limit are obtained as a function of the direction of motion and temperature by equilibrium Monte Carlo simulations. They contain moving vortex lattices, commensurate or incommensurate with the washboards periodicities, at low temperatures, moving smectics and moving liquids at higher ones. Finite-drive dynamical phase diagrams are then obtained by numerical solution of Langevin's equations. It is found that each dynamical phase originates from an infinite-drive limit phase with the same spatial symmetry that evolves continuously into finite-drive regions of the dynamical phase diagram. Dynamical transitions between moving commensurate or incommensurate lattices and moving liquids and between moving commensurate lattices and moving smectics are observed. Transverse pinning of vortices at low temperatures is found in regions of the dynamical phase diagrams where the dynamical phases are moving commensurate lattices or moving smectics.

74.60 Ge, 74.60 Jg

I. INTRODUCTION

A problem of current interest is the study of moving vortices interacting with arrays of pinning centers. Random arrays have received the most attention. However, periodic pinning arrays are also of interest. One reason is that they provide examples of dynamical phases and phase transitions, a subject not yet fully understood, where theoretical predictions can be tested in superconducting films with artificial defect lattices¹, and in Josephson junction arrays (JJA)².

In the case of moving vortices interacting with random pinning arrays, the dynamics is simpler when the driving force is large, in which case the velocity of the center of mass (CM) of the vortex array is also large. This situation was first considered by Schmid and Hauger³ who suggested that fast moving vortices average out the pinning potential and, consequently, order in a triangular lattice at low temperatures. In experiments⁴ and numerical simulations⁵ nearly triangular lattices are indeed observed at large CM velocity. Koshlev and Vinokur⁶ analyzed the effects of random pinning at large CM velocities on vortex displacement from the lattice equilibrium positions. They argued that it is equivalent to a

"shaking" temperature, inversely proportional to the CM velocity, that adds to the thermodynamic temperature, and predicted that dynamical melting of the moving vortex lattice takes place when the CM velocity is such that the combined temperature equals the equilibrium melting temperature. Recently, Gianmarchi and Le Doussal⁷ pointed out that this picture for the large CM velocities behavior breaks down, because the vortices order in a moving glass, rather than in a moving triangular lattice. The reason is that averaging of the pinning potential by the fast moving vortices is only partial. A static random pinning potential remains acting on the vortices in the frame of reference moving with the CM velocity (CM frame), and has non-trivial consequences on vortex order. These authors predict that the vortices move along static channels, on average parallel to the direction of drive, and are pinned on them with respect to a transverse force at zero temperature. This is referred to as transverse pinning. These predictions are in agreement with experimental and numerical results⁴.

In the case of vortices interacting with periodic pinning, the dynamics also simplifies in the limit of large driving forces. The question of what happens to the dynamical phases in this limit was first examined in recent

publications by the author⁸. These papers consider pinning by a square lattice of columnar defects (CD), and vortex motion in the $[0,1]$ (or $[1,0]$) direction. In Refs. 8 it is argued that moving vortices average the periodic pinning potential only in the direction of motion. It is also argued that the dynamical phases reduce to the equilibrium ones for vortices interacting with the periodic pinning potential averaged in the direction of motion, that is $[0,1]$, which is a washboard, periodic in the $[1,0]$ direction. This was shown to have non-trivial consequences for the dynamical phase diagram. The present paper studies further the limit of large drives for the model introduced in Ref. 8, allowing for arbitrary directions of vortex motion, and covering a wide temperature range. The dynamical phases in this limit are found to play a central role in determining the whole dynamical phase diagram.

Previous theoretical studies of vortices interacting with periodic pinning arrays are mostly numerical. Extensive studies of the zero-temperature vortex dynamics in systems with CD-lattices, carried out by several workers⁵, find a rather complex behavior, with many dynamical phases and phase transitions. A simpler finite-temperature behavior is found in JJA and films. Marconi and Dominguez⁹ carried out numerical simulations of square JJA, with the driving force along the $[1,0]$ (or $[0,1]$) direction. They find three dynamical phases: two moving vortex lattices and a moving liquid. In all three, the CM velocity is along the direction of drive. The lattices have the same spatial order, but differ from each other by the response to a force transverse to the direction of motion. One lattice, named transversely pinned vortex lattice, is pinned (transverse pinning), and the other, named floating solid, is unpinned. Dynamical melting of the floating solid into the liquid, and dynamical depinning from the pinned lattice to the floating solid are reported. Further work¹⁰ predicts transverse pinning only for driving forces along $[1,0]$ (or $[0,1]$), and verify it experimentally.

Work on films was carried out by Reichhardt and Zimányi¹¹ and by the author⁸. Both investigate vortices interacting with a square CD-lattice driven along the $[1,0]$, or $[0,1]$, directions, and consider the following vortex densities: 1 vortex per CD in Ref. 11; $5/4$ and 2 vortices per CD in Ref. 8. They find that the directions of vortex motion and drive coincide, and that the dynamical phase diagrams depend on the vortex density. For densities 1 and $5/4$ vortices per CD the dynamical phase diagrams are similar, with three dynamical phases: a moving lattice, commensurate with the pinning potential periodicity along the direction transverse to motion, a moving smectics and a moving liquid. Dynamical transitions between the commensurate lattice and the smectic and between the smectic and the liquid are found. In the commensurate lattice with 1 vortex per CD transverse pinning occurs¹¹. For 2 vortices per CD the only dynamical phases are an incommensurate lattice, essentially triangular, and a liquid, and dynamical melting between them takes place⁸. The present paper shows how these partic-

ular film results fit into a dynamical phase diagram that depends on the magnitude and direction of the driving force, and on the temperature.

The approach adopted here is similar to that used in Ref. 8. First the limit of high drives, where the dynamical phase diagrams are simpler, is studied in detail. Only then the paper proceeds to investigate the intermediate and low drives behavior.

The paper starts by considering Langevin's stochastic dynamical equations for a generic model for vortices interacting with periodic pinning at temperature T , and its behavior in the limit where the driving force magnitude approaches infinity. It is shown that in this limit these equations, written in the CM frame, describe vortices interacting between themselves and with a static effective pinning potential, equal to the average of the periodic pinning potential in the direction of motion. As a consequence, the dynamical phases reduce to the corresponding thermal equilibrium ones, which are hereafter referred to as infinite-drive phases. These phases are exact asymptotic limits of dynamical phases occurring in the dynamical phase diagram. The infinite-drive phases, being equilibrium phases, are distinguished from each other by the spatial order. Thus, dynamical phases with distinct spatial orders, one for each infinite-drive phase are expected to exist in finite-drive regions of the dynamical phase diagrams. The question is whether or not these dynamical phases exhaust the dynamical phase diagrams. The answer is found to be yes for the model studied in this paper, as well as for those investigated by Marconi and Dominguez⁹ and by Reichhardt and Zimányi¹¹.

Next, the paper studies numerically the London model for vortices interacting with a square CD-lattice introduced in Ref. 8. Two vortex densities, typical of the region where there are more vortices than CD ($B > B_\phi$), are considered: 2 vortices per CD ($B = 2B_\phi$) and $5/4$ vortices per CD ($B = 1.25B_\phi$). The model dynamical phase diagrams for these two densities are obtained numerically. First, the model infinite-drive phases and phase diagrams are obtained as a function of the temperature and direction of drive by equilibrium Monte Carlo simulations of the London model for vortices interacting with the above mentioned effective pinning potential. Then dynamical simulations of Langevin's equations describing the model dynamics are carried out. Based on the results of these simulations, the dynamical phases are identified and characterized, and the dynamical phase diagrams are obtained, as a function of the driving force magnitude and direction and of the temperature. The main findings are. i) All dynamical phases have a corresponding infinite-drive phase with the same spatial symmetry. The portion of the dynamical phase diagram occupied by each dynamical phase is found to extend continuously into large driving-force magnitude regions, where the dynamical phase is essentially identical to the corresponding infinite-drive one. ii) Directions of drive and vortex motion are in general distinct, leading to anisotropic V-I characteristics. iii) Existence of

two dynamical transitions. One, referred to as dynamical melting, between a moving incommensurate lattice and a moving liquid. Another, between a moving commensurate lattice or a moving smectic and a moving liquid. iv) Transverse pinning at low temperatures within regions of the dynamical phase diagram where the spatial symmetry is that of a moving commensurate lattice or a moving smectic, with vortex motion restricted to the $[\pm 1, 1]$ $[0, 1]$ and $[1, 0]$ CD-lattice directions.

A brief summary of the main numerical results is given next. The CD-lattice and the definitions of the coordinate system, CM velocity and driving force orientations are shown in Fig. 1. The model periodic pinning potential is shown in Fig. 2.a. The effective pinning potentials resulting from it are washboards, if motion is in the $[0, 1]$, $[1, 0]$ and $[\pm 1, 1]$ CD-lattice directions, and essentially a constant otherwise. The $[0, 1]$ and $[-1, 1]$ washboards are shown in Fig. 2.b and c. The $[1, 0]$ and $[1, 1]$ washboards follow from these by 90° rotation. The infinite-drive phases at low temperatures are found to be moving vortex lattices. For motion in the $[0, 1]$, $[1, 0]$ and $[\pm 1, 1]$ directions these lattices can be commensurate or incommensurate with the washboard's periodicity, as shown in Fig. 3. For motion in other directions the moving lattice is essentially triangular. Dynamical phase diagrams for driving forces oriented in the $[0, 1]$ and $[-1, 1]$ directions, in which case the directions of motion and drive coincide, are shown in Fig. 4. The low-temperature dynamical phase diagrams as a function of the driving force magnitude and direction are shown in Fig. 5. Within MIL regions in Fig. 5 a moving commensurate lattice exists, with the vortices ordered in a nearly triangular lattice. Dynamical melting lines separate it from a moving liquid. In the regions denoted MCL MCL45 and MSM in Fig. 5, transverse pinning occurs, with vortex motion is restricted to the $[-1, 1]$ direction. The vortices order in moving commensurate lattices within MCL and MCL45, with spatial symmetries equal to the infinite-drive phases with the same labels in Fig. 3. Within MSM the spatial order is that of a moving smectic, similar to the MSM phase for $B = 2B_\phi$ shown in Fig. 4.

This paper is organized as follows. The infinite-drive limit is considered in Sec. II. The London model and the numerical methods used to study it are presented in Sec. III. The simulation results are reported in Sec. IV. Finally, in Sec. V a discussion of the paper main results and comparison with earlier ones is presented, and the conclusions are stated.

II. INFINITE-DRIVE LIMIT

Here the limit of infinite driving force magnitudes is discussed for a generic model for vortices interacting with a CD-lattice.

The motion of N_v two-dimensional vortices is assumed to be governed by Langevin equations for massless par-

ticles, which for the l -th vortex reads¹²,

$$\eta \frac{d\mathbf{r}_l}{dt} = \mathbf{F}_l^{v-v} + \mathbf{F}_l^{v-cdl} + \mathbf{F}_d + \mathbf{\Gamma}_l, \quad (1)$$

where η is the friction coefficient,

$$\mathbf{F}_l^{v-v} = - \sum_{j \neq l=1}^{N_v} \nabla_l U^{v-v}(\mathbf{r}_l - \mathbf{r}_j), \quad (2)$$

is the force of interaction with other vortices, $U^{v-v}(\mathbf{r})$ being the vortex-vortex interaction potential in two-dimensions,

$$\mathbf{F}_l^{v-cdl} = -\nabla_l U^{v-cdl}(\mathbf{r}_l), \quad (3)$$

is the force of interaction with the CD-lattice, $U^{v-cdl}(\mathbf{r})$, being the respective potential, given by

$$U^{v-cdl}(\mathbf{r}) = \sum_{\mathbf{R}} U^{v-cd}(\mathbf{r} - \mathbf{R}), \quad (4)$$

where \mathbf{R} denotes the CD-lattice positions and $U^{v-cd}(\mathbf{r})$ is the interaction potential between a vortex and a single CD, \mathbf{F}_d is the driving force, and $\mathbf{\Gamma}_l$ is the random force appropriate for temperature T . In terms of Fourier transforms U_l^{v-cdl} can be written as

$$U^{v-cdl}(\mathbf{r}) = \sum_{\mathbf{Q}} U^{v-cd}(\mathbf{Q}) e^{i\mathbf{Q} \cdot \mathbf{r}}, \quad (5)$$

where \mathbf{Q} denotes the CD-lattice reciprocal lattice vectors, and $U^{v-cd}(\mathbf{Q})$ is the Fourier transform of $U^{v-cd}(\mathbf{r})$.

It is convenient to consider vortex motion in the frame moving with the CM. Let $\mathbf{r}'_l(t) = \mathbf{r}_l(t) - \mathbf{V}_{cm}t$ denote the l -th vortex position in the CM frame, \mathbf{V}_{cm} being the CM velocity, to be defined shortly. In the CM frame the vortex-CD lattice interaction, denoted here by $\mathbf{F}_l^{v-cdl}(t)$, depends explicitly on time, namely

$$\mathbf{F}_l^{v-cdl}(t) = \sum_{\mathbf{Q}} (-i\mathbf{Q}) U^{v-cd}(\mathbf{Q}) e^{i\mathbf{Q} \cdot \mathbf{r}'_l} e^{i\mathbf{Q} \cdot \mathbf{V}_{cm}t}, \quad (6)$$

The equation of motion for the l -th vortex in the CM frame reads,

$$\eta \frac{d\mathbf{r}'_l}{dt} = \mathbf{F}_l^{v-v} + \mathbf{F}_l^{v-cdl}(t) + \mathbf{F}_d - \eta \mathbf{V}_{cm} + \mathbf{\Gamma}_l, \quad (7)$$

The CM velocity is defined by the condition $\sum_1^{N_v} \langle d\mathbf{r}'_l(t)/dt \rangle_t = 0$, where $\langle \rangle_t$ denotes average over the random force distribution and over time. It follows from Eq. (7) that

$$\eta \mathbf{V}_{cm} = \mathbf{F}_d + \frac{1}{N_v} \sum_{j=1}^{N_v} \langle \mathbf{F}_j^{v-cdl}(t) \rangle_t. \quad (8)$$

In the limit $F_d \rightarrow \infty$, it follows from Eqs. (6) and (8) that $\mathbf{V}_{cm} = \mathbf{F}_d/\eta$, so that $V_{cm} \rightarrow \infty$ also. In this case, all Fourier components in $\mathbf{F}_l^{v-cdl}(t)$, Eq. (6), for

which $\mathbf{Q} \cdot \mathbf{V}_{cm} \neq 0$ oscillate fast, having a negligible effect on the vortex trajectory³, and $\mathbf{F}_l^{v-cdl}(t)$ reduces to the static force obtained by summing the Fourier components in $\mathbf{F}_l^{(v-cdl)}(t)$ with $\mathbf{Q} \cdot \mathbf{V}_{cm} = 0$, or $\mathbf{Q} \perp \mathbf{F}_d$, namely

$$\mathbf{F}_l^{v-cdl}(t) \rightarrow \sum_{\mathbf{Q} \perp \mathbf{F}_d} (-i\mathbf{Q}) U^{v-cd}(\mathbf{Q}) e^{i\mathbf{Q} \cdot \mathbf{r}'_l} \quad (9)$$

This force derives from the static effective pinning potential

$$U_\alpha^{eff}(\mathbf{r}'_\perp) = \sum_{\mathbf{Q} \perp \mathbf{F}_d} U^{(v-cd)}(\mathbf{Q}) e^{i\mathbf{Q} \cdot \mathbf{r}'_\perp}, \quad (10)$$

where \mathbf{r}'_\perp is the CM frame coordinate perpendicular to the direction of \mathbf{F}_d , and α the orientation of \mathbf{F}_d . This potential is equal to the average of U^{v-cdl} in the direction of motion (and drive). By definition, $U_\alpha^{eff}(\mathbf{r}'_\perp)$ is one-dimensional and periodic in the direction perpendicular to \mathbf{F}_d , if \mathbf{F}_d is oriented along one of the square CD-lattice directions and a constant otherwise, since no \mathbf{Q} is perpendicular to \mathbf{F}_d . The equations of motion in the CM frame, Eqs. (7), reduce then to those describing vortices interacting between themselves and with $U_\alpha^{eff}(\mathbf{r}'_\perp)$ at temperature T . Their long-time solutions are the corresponding equilibrium phases, called infinite-drive phases in this paper.

The infinite-drive limit establishes the exact asymptotic behavior $F_d \rightarrow \infty$ of the dynamical phase for given \mathbf{F}_d orientation and T . For finite F_d , the dynamical phase is expected to be close to the infinite-drive one with the same spatial symmetry for sufficiently large F_d . The condition for this to happen is that the vortex displacements in the CM frame caused by the pinning force oscillations in time, Eq. (7), during a time interval of the order of one-half period, are small compared with the vortex mean separation a_v . This means that for every \mathbf{Q} , such that $\mathbf{Q} \cdot \mathbf{F}_d \neq 0$,

$$Q | U^{(v-cd)}(\mathbf{Q}) | \frac{\pi}{\mathbf{Q} \cdot \mathbf{F}_d} \ll a_v. \quad (11)$$

III. MODEL AND NUMERICS

The model used in the numerical studies carried out here was introduced in Ref. 8. Vortices and CD are placed on a square lattice (space lattice), subjected to periodic boundary conditions with $N = 256 \times 256$ square primitive unit cells of dimensions $d \times d$. The CD-lattice is square, oriented parallel to space lattice and commensurate with it. The CD-lattice, the coordinate system and the angles defining the orientations of \mathbf{F}_d (α) and \mathbf{V}_{cm} (θ) are shown in Fig. 1.

The vortex has a core of linear dimension $d_v = 4d$ ($d_v \sim 2\xi(0)$), so that each vortex occupies 16 space-lattice sites. The vortex-vortex interaction potential

is a screened Coulomb one¹³, periodic in the space lattice, and characterized by the energy scale $J = (\phi_0^2 d_v / 32\pi^3 \lambda^2)$, where λ is the penetration depth. That is, $U^{v-v}(\mathbf{r})$ is the lattice Fourier transform of

$$U^{v-v}(\mathbf{k}) = 4\pi^2 J \frac{e^{-\frac{\kappa^2}{\kappa_c^2}}}{\kappa^2 + \Lambda^{-2}},$$

where $\kappa^2 = 4\sin^2(k_x d/2) + 4\sin^2(k_y d/2)$, k_x and k_y being the space lattice reciprocal lattice vectors components, $\kappa_c = 2\sin(\pi d/2d_v)$ is the vortex core cutoff in k-space, and Λ is the screening length ($\Lambda > \lambda$). The square CD-lattice has $N_{cd} = 8 \times 8$ sites, lattice constant $a_{cd} = 32d$. The interaction potential between a vortex and a single CD is chosen with depth $U^{v-cd}(\mathbf{r} = 0) = -J$, range $R_{cd} = 12d$ and a spatial dependence that gives square equipotentials and a pinning force of constant modulus $F_p = J/R_{cd}$, as shown in Fig. 2.a. The reciprocal CD-lattice vectors are

$$\mathbf{Q} = Q_1(n_1 \hat{\mathbf{x}} + n_2 \hat{\mathbf{y}}),$$

where $Q_1 = 2\pi/a_{cd}$, and $n_1, n_2 = -4, -3, \dots, 3$. It is found that the lattice Fourier transforms $U^{v-cd}(\mathbf{Q})$ are: $U^{v-cd}(0) = -0.19J$, $U^{v-cd}(\pm Q_1 \hat{\mathbf{x}}) = U^{v-cd}(\pm Q_1 \hat{\mathbf{y}}) = 0.10J$, $U^{v-cd}(\pm Q_1 [\hat{\mathbf{x}} \pm \hat{\mathbf{y}}]) = -0.06J$, and essentially negligible otherwise.

The model has the square lattice symmetry, so that the dynamical phase diagrams need only to be studied for \mathbf{F}_d orientations $0^\circ \leq \alpha \leq 45^\circ$.

The dynamical phases spatial order is obtained by calculating the time-averaged density-density correlation function, $P(\mathbf{r})$, which is proportional to the probability that a vortex is found at \mathbf{r} , given that there is one at $\mathbf{r} = 0$, and its Fourier transform, the structure function, $S(\mathbf{k})$. The motion of vortices is characterized by calculating the CM velocity, and the time-averaged velocity of each vortex.

Two types of numerical studies of the model are carried out. Equilibrium Monte Carlo simulations to obtain the infinite-drive phases, described in detail in Sec. IV A. Numerical integration of Langevin's equations to obtain the dynamical phase diagram as a function of F_d , α and T for two typical vortex densities: two vortices per CD and five vortices per four CD. These corresponds to the magnetic inductions $B = 2B_\phi$ and $B = 1.25B_\phi$, respectively, where $B_\phi = \phi_0/a_{cd}^2$ is the matching field, for which there is one vortex per CD. The numerical integration algorithm treats the vortex displacements as continuous during the run. In order to calculate the force acting on the vortices at each time step, the vortex positions are reduced to the nearest space lattice ones. The accuracy of this approximation increases with the number of space lattice sites occupied by each vortex, equal to 16 here. The numerical integrations are carried out at constant B , α and T , starting with a large F_d and the vortex positions initialized in a configuration appropriate for the infinite-drive phase. Subsequent runs, each with

a smaller F_d than the previous one, are carried out with the vortex positions initialized in the last configuration obtained in the previous run, until vortex motion can no longer be detected. In some cases, runs with F_d retracing the decreasing sequences are carried out in order to check for hysteresis. Typical runs consists of $\sim 0.4 - 1 \times 10^6$ integration steps at intervals $10^{-2}\tau$, where $\tau = \eta d^2/J$ is the natural time scale. In order to average the thermal force, the data reported here is the average over 10 repetitions of the same run, with different realizations of the random force.

IV. RESULTS

In this section the simulation results for the dynamical phase diagrams are reported. First in the infinite-drive limit, then for finite drives. In the figures presented here driving force magnitudes are measured relative to the single CD pinning force F_p , Sec. III; temperatures relative to the infinite-drive moving incommensurate lattice melting temperature T_m , Sec. IV A and center of mass velocity components relative to the components of $\mathbf{V}_d \equiv \mathbf{F}_d/\eta$.

A. Infinite-Drive Limit

The infinite-drive phase diagrams are obtained by equilibrium Monte Carlo simulations of the lattice London model with the pinning potential $U_\alpha^{eff}(r_\perp)$. It is found that for \mathbf{F}_d along $[0,1]$ ($\alpha = 0^\circ$) and $[-1,1]$ ($\alpha = 45^\circ$) the $U_\alpha^{eff}(r_\perp)$ are the washboards shown in Figs. 2b) and c). For \mathbf{F}_d along other lattice directions, the $U_\alpha^{eff}(r_\perp)$ are found to be very shallow washboards, because the $U^{(v-cd)}(\mathbf{Q})$ (Eq. (10)) are very small (Sec. III), and are considered as constant potentials in this paper. For example, the $U_\alpha^{eff}(r_\perp)$ for \mathbf{F}_d along the $[-1,2]$ direction ($\alpha = 26.6^\circ$), shown in Fig. 2.d has a well depth more than one order of magnitude smaller than that for $\alpha = 0^\circ$ and 45° shown in Figs. 2b) and c). For \mathbf{F}_d oriented in non-lattice directions, $U_\alpha^{eff}(r_\perp)$ is a constant. The corresponding low- T infinite-drive phases are as follows. For $\alpha = 0^\circ$ and 45° , they are vortex lattices (VL) commensurate or incommensurate with the one-dimensional periodicity, depending on B . The VL for $\alpha = 0^\circ$, are obtained here as a function of B , for $B \geq B_\phi$. Their density-density correlation functions, $P(\mathbf{r})$, are shown in Fig. 6. The commensurate lattices consist of identical vortex chains within each washboard channel, with neighbor chains displaced with respect to each other by half a chain period. There is a single chain for $B_\phi \leq B \leq B_1$, and two chains for $B_1 < B \leq B_2$. The values of B_1 and B_2 are found to be in the ranges $B_1 < 1.125B_\phi$ and $1.125B_\phi < B_2 < 1.375B_\phi$. A commensurate-incommensurate transition takes place for $B = B_{c-i}$ ($1.25B_\phi < B_{c-i} < 1.375B_\phi$). For $B > B_{c-i}$ the VL is incommensurate, and nearly triangular. For

$B = 2B_\phi$ and $B = 1.25B_\phi$ the $P(\mathbf{r})$ shown in Fig. 6 correspond, respectively, to the vortex lattices labeled MIL and MCL0 in Fig. 3. The effect of the one-dimensional periodic potential on the incommensurate lattice is to displace the vortices from the triangular lattice positions by a distance small compared to the lattice parameter¹⁴. It is found that, as expected, this effect is greater for B in the vicinity of B_{c-i} . This is evidenced by the behavior of $P(\mathbf{r})$ shown in Fig. 6. For $B = 1.375B_\phi$, $1.5B_\phi$, and $1.75B_\phi$, $P(\mathbf{r})$ has smeared spots centered in a nearly triangular grid, with smearing increasing with distance. For $B > 2B_\phi$, $P(\mathbf{r})$ has sharp spots, indicating that the displacements are negligible, and the VL is sharply defined.

The two B values studied in this paper, $B = 2B_\phi$ and $B = 1.25B_\phi$, are typical of parameter regions far from commensurate-incommensurate transitions, both for $\alpha = 0^\circ$ and $\alpha = 45^\circ$, where the VL are sharply defined. The infinite-drive phase diagrams in these cases are as follows. For $\alpha = 0^\circ$ and 45° the VL are shown in Fig. 3. These are referred to in this paper as moving incommensurate lattices (MIL) and moving commensurate lattices, with distinct vortex configurations labeled MCL, MCL0 and MCL45, as shown in Fig. 3. For $0^\circ < \alpha < 45^\circ$, the VL are incommensurate and nearly triangular. It is found that the incommensurate lattices for the same B , but different α , cannot be distinguished from each other. Hereafter all incommensurate lattices are referred to as moving incommensurate lattices (MIL).

The T -dependence of the infinite-drive phases (at constant α is found to be as follows: the moving incommensurate lattices (MIL) melts into a moving vortex liquid (MLQ) at $k_B T_m = 0.09J$, for both B . For $B = 2B_\phi$ the moving commensurate lattice (MCL) changes into a moving smectic (MSM) at $T_{mcl}/T_m = 1.4$ and the moving smectic (MSM) changes into a moving liquid (MLQ) at $T_{msm}/T_m = 1.8$. For $B = 1.25B_\phi$ the moving commensurate lattices, MCL0 and MCL45, change into a moving smectic (MSM) at $T_{mcl0}/T_m = 1.2$ and $T_{mcl45}/T_m = 1.7$, respectively.

B. Finite Drives

First the results for \mathbf{F}_d oriented along the high symmetry directions $[0,1]$ ($\alpha = 0^\circ$), and $[-1,1]$ ($\alpha = 45^\circ$) are presented. In these cases the directions of motion and drive coincide ($\theta = \alpha$) all the way down to the F_d values where $V_{cm} = 0$. Next results for $0^\circ < \alpha < 45^\circ$ are discussed.

1. Drive along $\alpha = 0^\circ$ and $\alpha = 45^\circ$

Dynamical phase diagrams (F_d vs. T) are shown in Fig. 4. For $B = 2B_\phi$, $\alpha = 0^\circ$, only two dynamical phases exist: a moving incommensurate lattice (MIL) and a

moving liquid (MLQ), separated by a dynamical melting line, as shown in Fig. 4. The dynamical phase diagrams for both B , $\alpha = 45^\circ$, and for $B = 1.25B_\phi$, $\alpha = 0^\circ$, are similar to one another, containing three phases: a moving commensurate lattice (MCL for $B = 2B_\phi$, MCL0 and MCL45 for $B = 1.25B_\phi$) a moving smectic (MSM) and a moving liquid. Only the dynamical phase diagrams for $B = 2B_\phi$, $\alpha = 45^\circ$, and $B = 1.25B_\phi$, $\alpha = 0^\circ$ are shown in Fig. 4. That for $B = 1.25B_\phi$, $\alpha = 45^\circ$, is similar. In the temperature range covered by Fig. 4 the transitions between the moving smectics and moving liquids do not appear. The low T properties of the $\alpha = 0$ phase diagrams are studied in detail in Ref. 8. In Fig. 4 typical $P(\mathbf{r})$ at large F_d/F_p for the above described phases are shown. It is found that the dynamical phases at large F_d/F_p essentially coincide with the corresponding infinite-drive ones. The dynamical phase diagrams in Fig. 4 show clearly that each dynamical phase originates from the infinite-drive one with the same spatial symmetry that evolves continuously into finite drive regions.

For $B = 2B_\phi$ the vortices freeze at low T into the zero-drive lattice (ZDL in Fig. 1) below the dotted lines in Fig. 4. In this case the phase diagrams show little irreversibility. That is, if F_d is increased starting from the zero drive lattice essentially the same results are obtained. For $B = 1.25B_\phi$ the vortices do not freeze at low T into the equilibrium zero drive lattice, but remain in a metastable state, similar to the moving smectic, down to very small F_d . The zero-drive lattice in this case is found to be a complex VL, commensurate with the full CD-lattice potential, but with many vortices per unit cell. However, if F_d is increased starting from the metastable state, little hysteresis is found.

The transition lines show in Fig. 4 indicate the existence of two regimes for the dynamical transitions. One, for large F_d , where the transition temperature depends weakly on F_d , being close to its equilibrium values in the infinite-drive limit, showing that the transitions are driven by thermal fluctuations. The other, at small F_d , where the transition force depends weakly on T , being close to the limit value of F_d as $T \rightarrow 0$, indicating that the transitions are driven by vortex vibrations, caused by motion in the periodic pinning potential. The latter mechanism is similar to vortex 'shaking', proposed in Ref. 6 for random pinning, but a 'shaking' temperature cannot be defined.

As discussed next, the commensurate VL (MCL, MCL0 and MCL45) show transverse pinning at low T . This may be expected because for $\alpha = 0^\circ$ and $\alpha = 45^\circ$, \mathbf{V}_{cm} remains parallel to \mathbf{F}_d . In all these cases, according to Eq. (6), the effective pinning potential ($U_\alpha^{eff}(r_\perp)$) acts on the moving vortices for all F_d , not only in the $F_d \rightarrow \infty$ limit. The commensurate phases are pinned by $U_\alpha^{eff}(r_\perp)$ with respect to a small force along the direction defined by r_\perp .

2. Drives along $0^\circ < \alpha < 45^\circ$

The dynamical phases found in this range of driving-force orientations have the same spatial symmetries as those described in Secs. IV A and IV B 1 and are referred to in what follows by the same nomenclature.

The F_d vs. α dynamical phase diagrams at low- T are shown in Fig. 5. Both have two dynamical transition lines. One, referred to here as dynamical melting line, separating a moving incommensurate lattice (MIL) and a moving liquid (MLQ). Another separating a moving commensurate lattice (MCL for $B = 2B_\phi$ and MCL45 for $B = 1.25B_\phi$) or a moving smectic (MSM) for $B = 2B_\phi$ and a moving liquid. Within the moving commensurate lattice and moving smectic regions transverse pinning occurs, with the vortices moving along the $[-1,1]$ direction. The transition line in the $B = 2B_\phi$ dynamical phase diagram from the moving commensurate lattice (MCL) and the moving smectic (MSM) occurs with the vortices moving in the $[-1,1]$ direction, and is essentially identical to that for $\alpha = 45^\circ$ discussed in Sec. IV B 1

For clarity of presentation, the dynamical phase diagrams of Fig. 5 do not show the F_d vs. α line representing the cessation of vortex motion at small F_d . It is found that the behavior is similar to that for $\alpha = 0^\circ$ and 45° discussed in Sec. IV B 1. For $B = 2B_\phi$ the vortices freeze in the zero-drive lattice (ZDL) shown in Fig. 1 for all α . For $B = 1.25B_\phi$ freezing of the vortices occurs in a metastable state which change somewhat with α .

The evidence leading to the construction of the dynamical phase diagrams in Fig. 5 is summarized in Figs. 7, 8, 9, and 10, where the dependencies of the spatial order and \mathbf{V}_{cm} on F_d , along lines of constant α in Figs. 5.a and b, are shown. The evolution with F_d of $S(\mathbf{k})$ is shown in Figs. 7 and 8 along the $\alpha = 35^\circ$ line for $B = 2B_\phi$, and along the $\alpha = 40^\circ$ line for $B = 1.25B_\phi$. The changes occurring in $S(\mathbf{k})$ shown in these figures when F_d crosses one of the transition lines are typical of those occurring across the same line at different α . In Figs. 9 and 10 the direction of motion (θ) vs. F_d curves are shown for various α . Also shown in is the component of \mathbf{V}_{cm} perpendicular to the $[-1,1]$ direction, denoted V_\perp , as a function of F_d . This quantity is proportional to the voltage difference between contacts placed perpendicular to the $[-1,1]$ direction. In Figs. 9 and 10. V_\perp is measured relative to the component of $\mathbf{V}_d \equiv \mathbf{F}_d/\eta$ perpendicular to the $[-1,1]$ direction, denoted by $V_{d\perp}$.

The detailed properties of the dynamical phase diagrams shown in Fig. 5 are as follows.

i) *Dynamical Melting*. The dynamical melting lines extend from $\alpha = 0^\circ$ to $\alpha = 45^\circ$. For $B = 2B_\phi$ it touches the $\alpha = 0^\circ$ -axis at the F_d value where the dynamical melting takes place for $\alpha = 0^\circ$ and $T/T_m = 0.83$ (Fig. 4). It does not touch the $\alpha = 45^\circ$ axis for both B and the $\alpha = 0^\circ$ axis for $B = 1.25B_\phi$, because the dynamical phases in these axes are not moving incommensurate lattices, as discussed in Sec. IV A. These result of (Fig. 5) show that,

for both B , the moving incommensurate and commensurate lattices are separated by a moving liquid, at least up to the highest F_d studied here. However, in the infinite-drive phase diagram there is no moving liquid at these temperatures. It is unclear how the disappearance of the moving liquid as $F_d \rightarrow \infty$ takes place.

The θ vs. F_d curves in Figs. 9 and 10 show that in the moving incommensurate lattice (MIL) the directions of drive and vortex motion are approximately equal ($\theta \simeq \alpha$), and that the melting transition is reflected in this curve by a change in slope. For $B = 2B_\phi$ this change is sharp, with θ increasing rapidly towards $\theta = 45^\circ$ as F_d decreases. For $B = 1.25B_\phi$ the same is true, as long as $\alpha \gtrsim 20^\circ$, while for smaller α the moving liquid θ slowly approaches $\theta = 0^\circ$ as F_d decreases.

It is found that the moving liquids are anisotropic, particularly when θ is close to $\theta = 45^\circ$. This is evidenced by the $S(\mathbf{k})$ panels in Fig. 7 for $F_d/F_p = 2.0$, and in Fig. 8 for $F_d/F_p = 2.5$ and $F_d/F_p = 0.75$, where a pair of peaks at $\mathbf{k} = \pm Q_1(\hat{\mathbf{x}} + \hat{\mathbf{y}})$ occurs. These peaks result from a modulation in the vortex density along $[1,1]$, with wavelength $\sqrt{2}a_{cd}$, due to vortex motion being predominantly along the $[-1,1]$ direction ($\theta \sim 45^\circ$, see Figs. 9 and 10), which favor concentration of vortices around lines in the $[-1,1]$ direction connecting the CD-lattice potential minima (Fig. 2.a).

ii) *TransversePinning*. The results shown in Figs. 9 and 10 indicate that in the regions where the spatial order is that of a moving commensurate lattice, or a moving smectic for $B = 2B_\phi$, transverse pinning occurs, and vortex motion is restricted to the $[-1,1]$ direction. This is seen in Figs. 9 and 10, where $V_\perp = 0$ and $\theta = 45^\circ$ in the F_d range of moving commensurate lattices or smectics, and the distribution of individual vortices direction of motion is sharply peaked around $\theta = 45^\circ$ (Fig. 9, inset). In the literature, transverse pinning is usually discussed in terms of the \mathbf{F}_d component perpendicular to the direction of motion needed to depin the vortices. For the results shown in Fig. 5 this quantity, denoted here by $F_{\perp c}$, can be obtained from the transition lines between the moving commensurate lattices, or smectics, and the moving liquid by $F_{\perp c} = F_d \sin(45^\circ - \alpha)$, where F_d and α are taken at these lines. These results also show that the moving commensurate and smectic regions evolve continuously from the corresponding infinite-drive phases. As pointed out in Sec. IV A, transverse pinning can be anticipated when the infinite-drive phase is a commensurate lattice. In the cases where this lattice is a single-chain one, $\alpha = 45^\circ$ both B (Fig. 3), the depinning force can be estimated as being that for a single vortex, which is equal to the maximum force exerted by the $\alpha = 45^\circ$ washboard (Fig. 2.c). The value of the maximum force is found to agree, within the simulation errors, with $F_{\perp c}$ obtained from the data shown in Fig. 5 at large F_d . In the case $B = 1.25B_\phi$, it is expected that a moving commensurate lattice region with spatial symmetry MCL0 occurs near $\alpha = 0^\circ$. This region is not observed for $T/T_m = 0.89$,

used in Fig. 5, but lower T results indicate that it exists, and is restricted to the immediate vicinity of $\alpha = 0^\circ$. This may result from a very small transverse depinning force for the MCL0 moving commensurate lattice, due to its two-chain structure. This makes it difficult to obtain accurate results for this region, and it will not be discussed further in this paper.

The temperature dependence of the dynamical phase diagrams is as follows. For temperatures lower than those of Fig. 5 the dynamical phase diagrams are similar. The dynamical melting lines are shifted to lower F_d , similarly to what happens for $B = 2B_\phi$ and $\alpha = 0^\circ$ (Fig. 4). Transverse pinning in the moving commensurate lattices also occurs, as evidenced by the V_\perp vs. F_d curves shown in Fig. 11. For higher temperatures several changes are observed. The dynamical melting lines also exist, shifted to larger F_d , provided T does not exceed the infinite-drive melting temperature T_m . When $T > T_m$ the moving incommensurate lattices do not exist, only moving liquids.

As well known⁷, transverse pinning in the moving commensurate lattices or smectics only exists, strictly speaking, at $T = 0$. At finite T thermal excitation of lattice defects lead to flux motion away from the $[-1,1]$ direction, giving rise to a finite V_\perp . The regions of transverse pinning found in the present simulations occur because the thermally excited V_\perp is smaller than the simulation resolution. In experiments, where the resolution is also finite, these regions may also be present. The T dependence of the V_\perp vs F_d curves are shown in Fig. 11. For $B = 2B_\phi$ transverse pinning is found in the moving commensurate lattice and moving smectics at temperatures above T_m , whereas for $B = 1.25B_\phi$ it disappears at lower temperatures.

V. DISCUSSION

The results described in Sec. IV reveal the important role played by the infinite-drive phases. They show that all dynamical phases originate from infinite-drive phases with the same spatial symmetry that evolve continuously into regions of finite drives.

The results obtained by Reichhardt and Zimányi¹¹ for vortices in films interacting with a square CD-lattice, driven in the $[1,0]$ direction, at $B = B_\phi$, show a similar behavior. The infinite-drive phase diagram was not considered in this paper, but can be identified with the reported dynamical phase diagrams at high drives. It consists, in the terminology adopted here, of the following phases. A moving commensurate lattice at low T , with single-chain structure similar to that shown in Fig. 6 for $B = 1.125B_\phi$ rotated by 90° , a moving smectic at intermediate T , and a moving liquid at high T . The dynamical phase diagram reported in Ref. 11 shows that these three phases exist in continuous regions of the driving force vs. T phase diagrams that extend from high to low drives. This phase diagram is similar to those found

here for $B = 1.25B_\phi$, $\alpha = 0^\circ$ and 45° , and for $B = 2B_\phi$ $\alpha = 45^\circ$ (Sec. IV B 1).

For vortices in JJA, driven in the $[1,0]$ direction, the dynamical phase diagram reported by Marconi and Dominguez⁹ also show dynamical phases existing in continuous regions of the driving force vs. T plane that extend from high to low drives. However it is not possible to identify the infinite-drive phases from the data reported in the paper.

Some studies of vortices interacting with CD-lattices at $T = 0$ ⁵ find dynamical phases and phase transitions similar to the ones reported in this paper and in Ref. 11. Examples are tranverse pinning, moving commensurate and incommensurate lattices and dynamical transitions between them. However, these studies probe dynamical behavior different from the finite-temperature ones discussed here. At finite temperatures, the vortices relax after sufficient long times to a steady state, identified as the dynamical phase, that is unique as far as the probability distribution is concerned¹⁵. Accordingly, dynamical phase changes caused by varying the driving force, the temperature, or both, are reversible. This is not necessarily the case at $T = 0$. However, in numerical studies, irreversibility appears due to insufficient run times to reach the steady state, particularly when relaxation times are very large. This occurs in several circumstances, such as low temperatures, or vicinity of dynamical phase changes. In the simulations reported in this paper low temperatures are avoided. Some simulation runs were performed cycling the driving force magnitude from a large value to a small one and back. Small hysteresis is found near dynamical phase transitions.

In conclusion, the approach adopted in this paper to construct the dynamical phase diagrams, starting from the infinite-drive ones, provides a simple method, based on equilibrium statistical mechanics, to identify dynamical phases spatial order, and to predict dynamical phase transitions. It is expected that this method is applicable to a large class of periodic pinning potentials and vortex densities. The reasons are that the effective pinning potentials resulting from averaging physically reasonable periodic pinning potentials in the direction of motion are, as those discussed in Sec. IV A, essentially constant for most directions, and one-dimensional and periodic for a few particular ones. This predicts the existence, for $B \geq B_\phi$, of moving lattices, commensurate or incommensurate with the effective pinning potential periodicity, moving smectics and moving liquids, similar to the ones reported here, and of dynamical phase transitions between them. For $B < B_\phi$ the moving lattices may be different, particularly at low vortex densities, where the commensurate infinite-drive phases are not expected to retain the simple chain structure found here for the $B \geq B_\phi$ ones. However, the close relationship between the dynamical phase diagrams and the infinite-drive ones are still valid, as evidenced by the JJA results of Ref. 9. The dynamical phases obtained by this method do not, in general, exhaust the dynamical phase diagram. One

known type of dynamical phase that has no corresponding infinite-drive phase is that in which some vortices are pinned by the periodic potential and others are moving. These are found at low drives in some $T = 0$ simulations for $B > B_\phi$ ⁵. No such phases are found in the present simulations nor in Refs. 5,9. The details of how the dynamical phases and dynamical phase transitions predicted by the method proposed here fit into the dynamical phase diagram for each particular model and vortex density depends in a complicated way on the model parameters, and has to be determined in each case.

ACKNOWLEDGMENTS

Research supported in part by CNPq, CAPES, FAPERJ and FUJB.

* e-mail:gmc@if.ufrj.br

- ¹ A.N. Lykov, Adv. Phys. **42**, 263 (1993) V.V. Metlushko *et al.*, Sol. St. Comm. **91**, 331 (1994); M. Baert *et al.*, Phys. Rev. Lett. **74**, 3269 (1995); E. Rossel *et al.*, Phys. Rev. B **53**, R2983 (1996); V.V. Moshchalkov *et al.*, *ibid.* **54**, 7385 (1996); **57**, 3615 (1998); K. Harada *et al.*, Science **274**, 1167 (1996). J.-Y. Lin *et al.*, Phys. Rev. B **54**, R12717 (1996). L. Van Look *et al.*, *ibid.* **60**, 6998 (1999). B. Y. Zhu *et al.*, *ibid.* **64**, 012504 (2001)
- ² R. S. Newrock *et al.*, Solid State Phys. **54**, 263 (2000).
- ³ A. Schmid and W. Hauger, J. Low Temp. Phys. **11**, 667 (1973).
- ⁴ R. Thorel *et al.*, J. Phys. (Paris) **34**, 447 (1973); S. Bhattacharya and M.J. Higgins, Phys. Rev. Lett. **70**, 2617 (1993); U. Yaron *et al.*, Phys. Rev. Lett. **73**, 2748(1994); Nature (London) **376**,753 (1995); A. Duarte *et al.*, Phys. Rev. B **53**, 11336 (1996). F. Pardo *et al.*, Phys. Rev. Lett. **78**, 4633 (1997); M. Marchevsky *et al.*, *ibid.* **78**, 531 (1997).
- ⁵ C. Reichhardt *et al.*, Phys. Rev. B **54**, 16108 (1996); *ibid.* **57**, 7937 (1998); *ibid.* **58**, 6534 (1998); Phys. Rev. Lett. **78** 2648 (1997); *ibid.* **82** 414 (1999); H. Fangohr, S.J. Cox, and P.A.J. de Groot, Phys. Rev. B **64**, 064505 (2001).
- ⁶ A.E. Koshelev and V.M Vinokur, Phys. Rev. Lett. **73**, 3580 (1994).
- ⁷ T. Giamarchi and P. Le Doussal, Phys. Rev. Lett. **76**, 3408 (1996); Physica C **282**,363(1997); Phys. Rev. B **57**, 11356 (1998).
- ⁸ G. Carneiro J. Low Temp. Phys. **117**, 1323 (1999); Phys. Rev. B **61**, R 14661 (2000).
- ⁹ V.I. Marconi and D. Dominguez, Phys. Rev. Lett. **82**, 4922 (1999); Phys. Rev B **63**, 174509 (2001).
- ¹⁰ V.I. Marconi *et al.*, Phys. Rev. B **62**, 4096 (2000).
- ¹¹ C. Reichhardt and G.T. Zimányi, Phys. Rev. B **61**, 14354 (2000).
- ¹² E.H. Brandt, Rep. Prog. Phys. **58**, 1465 (1995).

¹³ P. Minnhagen Rev. Mod. Phys. **59**, 1001 (1987)

¹⁴ See eg. D.R. Nelson, *Phase transitions and Critical Phenomena*, Vol. 7, C. Domb and M.S. Green, eds. (Academic Press,1983), Chap. 1.

¹⁵ See eg. H. Risken, *The Fokker-Planck Equation. Methods of Solution and Applications*. (Springer,1989), Chap. 6.

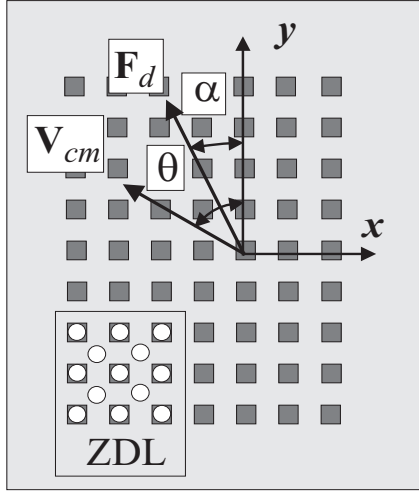


FIG. 1. Columnar defect-lattice and definitions of coordinate system, CM velocity (\mathbf{V}_{cm}) and driving force (\mathbf{F}_d) orientations. Inset: low- T equilibrium vortex state at zero-drive for $B = 2B_\phi$ (ZDL).

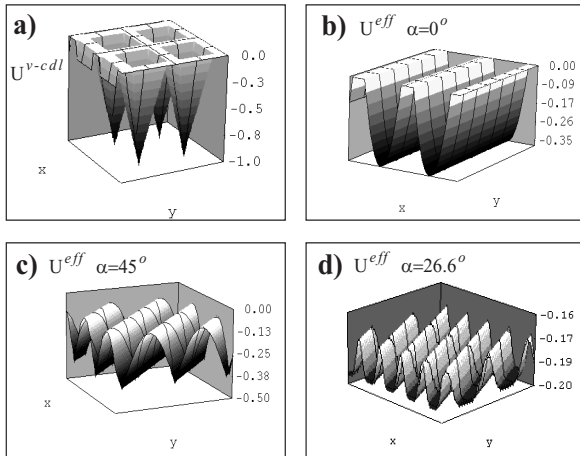


FIG. 2. a) Columnar defect-lattice pinning potential. b-d) Effective pinning potentials for motion in: b) [0,1] direction ($\alpha = 0^\circ$), c) [-1,1] direction ($\alpha = 45^\circ$), and d) [-1,2] direction ($\alpha = 26.6^\circ$). Potentials in units of the single CD potential well depth (J).

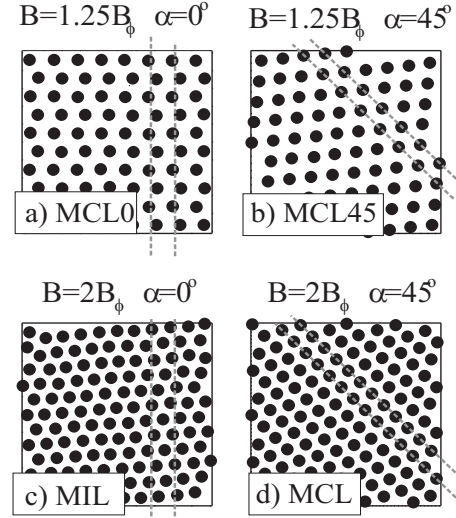


FIG. 3. Vortex positions in low- T infinite-drive phases. Dashed gray lines indicate minima of U_α^{eff} shown in Figs.2.b and 2.c. Nomenclature: moving commensurate lattices: a) MCL0, b) MCL45 and d) MCL. Moving incommensurate lattices: c) MIL

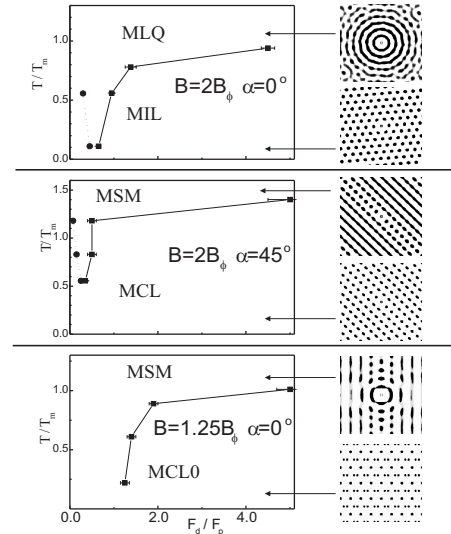


FIG. 4. Dynamical phase diagrams for drives along [0,1] ($\alpha = 0^\circ$) and [-1,1] ($\alpha = 45^\circ$). Panels: density-density correlation functions $P(\mathbf{r})$ at high drives ($\mathbf{r} = 0$ is at the panel's center). Nomenclature: MLQ=moving liquid, MSM=moving smectic. Others as in Fig.3. Dotted lines in the pannels for $B = 2B_\phi$ indicate where vortex motion stops.

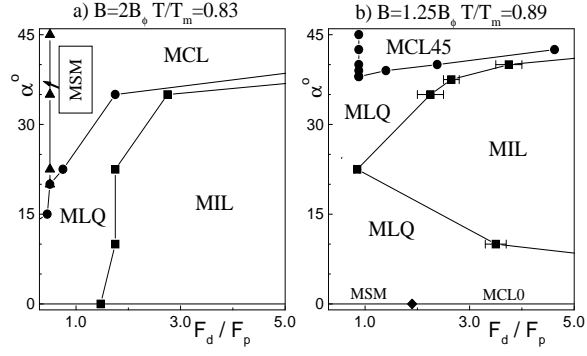


FIG. 5. Dynamical phase diagrams for $T = \text{constant}$. Dynamical phases named as in Figs. 3 and 4.

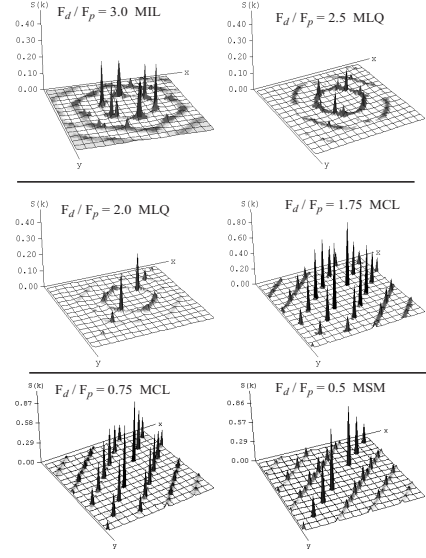


FIG. 7. Dependence of the structure function, $S(\mathbf{k})$, for $B=2B_\phi$ and $T/T_m=0.83$ on driving force, F_p , along the $\alpha=35^\circ$ line in Fig.5.a. Spatial symmetries named as in Fig.3 and 4.

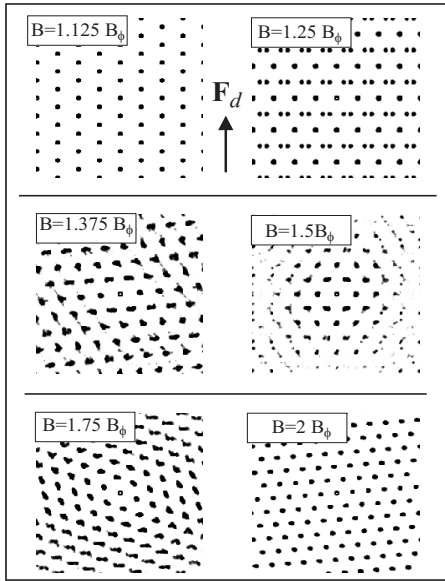


FIG. 6. Density-density correlation functions, $P(\mathbf{r})$ ($\mathbf{r}=0$ is at the panel's center), for low- T infinite-drive phases for motion in the $[0,1]$ ($\alpha=0^\circ$) direction as a function of B .

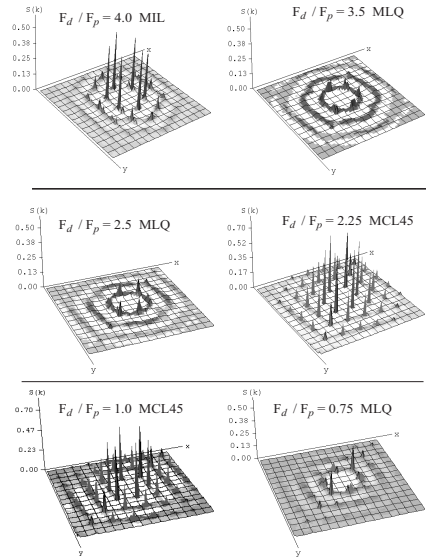


FIG. 8. Dependence of the structure function, $S(\mathbf{k})$, for $B=1.25B_\phi$ and $T/T_m=0.89$ on driving force, F_p , along the $\alpha=40^\circ$ line in Fig.5.b. Spatial symmetries named as in Fig.3 and 4.

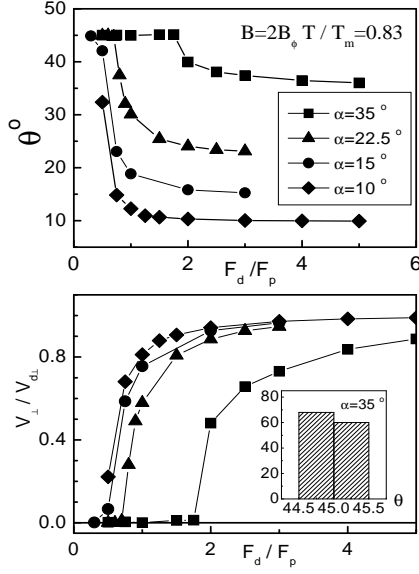


FIG. 9. Center of mass velocity direction (θ) and component perpendicular to the $[-1,1]$ direction, V_{\perp} , vs. driving force magnitude along lines of constant α in Fig.5.a. Inset: histogram for the distribution of vortices direction of motion (θ) for $\alpha = 35^\circ$ and $F_d/F_p = 1.5$.

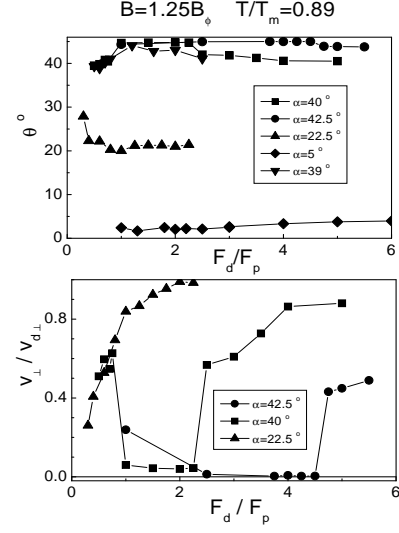


FIG. 10. Center of mass velocity direction (θ) and component perpendicular to the $[-1,1]$ direction, V_{\perp} , vs. driving force magnitude along lines of constant α in Fig.5.b.

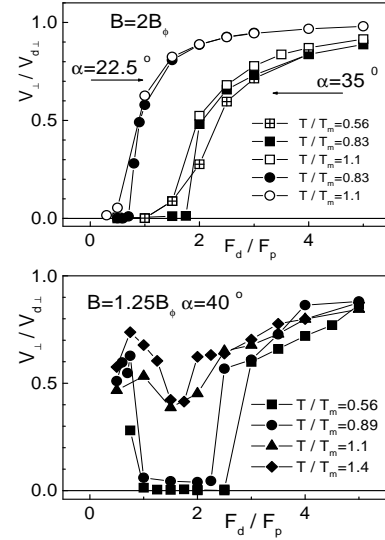


FIG. 11. Component of CM velocity perpendicular to $[-1,1]$, V_{\perp} , vs. driving force magnitude along lines of constant α and at constant temperatures.